



FAKULTÄT FÜR PHYSIK
PHYSIKALISCHES PRAKTIKUM FÜR FORTGESCHRITTENE
PRAKTIKUM MODERNE PHYSIK

Gruppe Nr.

Kurs: **Mo1** **Mo2** **Mi3**
zutreffendes bitte ankreuzen

WS24/25

aktuelles Semester angeben

Versuch: Compton scattering

Namen:

Assistent:

durchgeführt am:

Protokollabgabe am:

vom Betreuer auszufüllen

Note gesamt	<input type="checkbox"/>	<input checked="" type="checkbox"/>	<input type="checkbox"/>
Anerkannt:	<input type="checkbox"/>		
	(Datum Unterschrift)		
Datum Rückgabe:	<input type="checkbox"/>		
Bemerkung:	<input type="checkbox"/>		

Contents

1	Theoretical principles	3
1.1	Compton scattering	3
1.2	Cross section	4
1.2.1	In Classical Mechanics	4
1.2.2	In Quantum Mechanics	4
2	Experimental Setup	5
2.1	Radiation sources	5
2.2	Detector	5
2.3	Targets	5
3	Execution and evaluation	7
3.1	Task 1 - Energy calibration and efficiency calculation	7
3.1.1	Energy calibration	7
3.1.2	Efficiency calculation	7
3.2	Task 2 - Measurement of the differential effective cross section	9
3.3	Task 3 - Measurement of the energy shift and estimation of the rest energy of the electron	10
3.4	Task 4 - Measurement of the dependence of the effective cross section on the atomic number	12
	Sources	14

1 Theoretical principles

1.1 Compton scattering

The Compton effect is a phenomenon in quantum mechanics where γ -quanta, usually photons, scatter off free charged particles, usually electrons, resulting in a change in the photon's energy and direction. It allows γ -quanta to be detected and their energy measured. If the charged particles are at rest or have low kinetic energy compared to that of the photon, the photon will lose energy. This means that after the collision, the photon will have a longer wavelength and a lower frequency. This energy is then transferred to the charged particle in the form of kinetic energy. As an example, consider a photon with energy E and an electron at rest with energy E_0 . Upon interaction, the photon will have an energy $E' < E$, and the electron will have an energy $E_e > E_0$. Using the conservation of energy

$$E + E_0 = E_e + E' \quad (1.1)$$

and the momentum theorem

$$c^2 p^2 = E_e^2 - E_0^2 = E^2 + (E')^2 - 2E \cdot E' \cdot \cos \theta, \quad (1.2)$$

it is possible to calculate the energy of the photon and the kinetic energy of the electron after the interaction:

$$E'(\theta, E) = \frac{E}{1 + \frac{E}{E_0}(1 - \cos \theta)} \quad (1.3)$$

$$E_{\text{kin}}(\theta, E) = E - E'(\theta, E) = \frac{\frac{E^2}{E_0}(1 - \cos \theta)}{1 + \frac{E}{E_0}(1 - \cos \theta)} \quad (1.4)$$

As can be seen, the change in energy during scattering, also called the Compton shift, depends on the initial energy of the photon. The larger E in relation to E_0 , the larger the shift. The Compton effect is only noticeable when E is comparable with E_0 . Additionally, it depends on the scattering angle θ as well. The larger the angle, the more energy will be transferred. For very small angles such that $\theta \rightarrow 0$, the charged particle will not receive any energy

$$E_{\text{kin}}(\theta \rightarrow 0, E) = \frac{\frac{E^2}{E_0}(1 - 1)}{1 + \frac{E}{E_0}(1 - 1)} = 0, \quad (1.5)$$

whereas for an angle $\theta = \pi$ (backscattering), the energy transfer is maximized:

$$E_{\text{kin}}(\pi, E) = \frac{\frac{E^2}{E_0}(1 - (-1))}{1 + \frac{E}{E_0}(1 - (-1))} = \frac{E}{\frac{E_0}{2E} + 1} < E. \quad (1.6)$$

Naturally, even the maximum kinetic energy of the electron is less than the initial energy of the photon, since the photon keeps part its initial energy.

1.2 Cross section

1.2.1 In Classical Mechanics

In the classical context, the cross section σ describes the apparent area that a particle presents for another to collide with it. For example, if particles, considered as spheres, are launched toward a target, the cross section would be the effective area that determines whether the incoming particles interact with the target. In more complex collisions, such as those involving charged particles, the cross section may depend on factors like the forces between them and their trajectories.

1.2.2 In Quantum Mechanics

In quantum mechanics, the concept is similar, but the cross section incorporates quantum phenomena such as wave interference and the effects of the wave function. Here, the cross section is not just a physical area but a measure of the probability of interaction. For n target particles within an area F , the probability of occurrence is given by

$$P_n = n \cdot \frac{\sigma}{F}. \quad (1.7)$$

The total cross section, which covers all the reactions of the output channel regardless of the direction taken by the reaction products, is typically defined by

$$\sigma = \frac{\text{Particle flux, by which the incident flux decreases}}{\text{incident particle flux} \otimes \text{number of target particles per area}}. \quad (1.8)$$

Similarly, the differential cross section $\frac{d\sigma}{d\Omega}$ describes how the probability of an interaction or scattering varies as a function of the solid angle $d\Omega$. In other words, it indicates how many particles are scattered in a particular direction (i.e., within a small angle) rather than in all possible directions. Mathematically, its general definition is analogous to that of the total cross section:

$$\frac{d\sigma}{d\Omega} = \frac{\text{Particle flux per solid angle, by which the incident flux decreases falling in } d\Omega}{\text{incident particle flux} \otimes \text{number of target particles per area}}. \quad (1.9)$$

2 Experimental Setup

The experimental setup comprises a primary radiation source, three calibration sources, a rotating detector, and an array of targets. The entire assembly is shielded by multiple layers of lead blocks to minimize background radiation and to protect the people around the experiment.

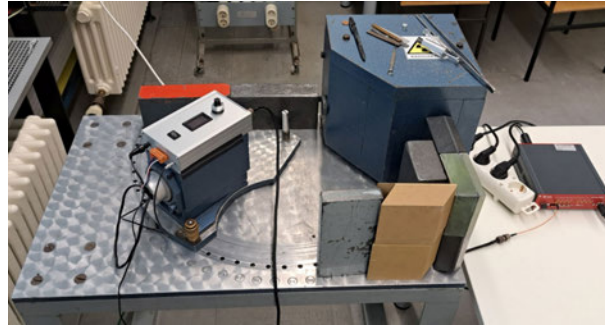


Figure 2.1: The main source is embedded in a blue lead block, the detector is positioned to the left of the source, and the targets are lying on the blue block. Lead shielding consisting of multiple loose blocks protects the setup and the people around it.

2.1 Radiation sources

The three sources, ^{137}Cs , ^{22}Na and ^{60}Co , were used to calibrate the detector. These isotopes are chosen because their emission spectra, in particular their photopeaks, are well-known, enabling precise calibration.

The main source used in Task 2 to 4 is a stronger ^{137}Cs -source. As can be seen in Figure 2.1, the source is positioned within a shielded housing which allows radiation to emerge through a narrow window, ensuring a γ -beam along a fixed axis.

2.2 Detector

The detector system consists of a CeBr_3 scintillator, a photomultiplier and a digitizer. Deflected γ -rays are first captured by the scintillator, in which their energy is converted into optical photons corresponding to their initial energy. These photons are then further amplified by the photomultiplier and converted into a electric pulse. The pulse is then digitized and transferred to a computer for storage and analysis of the captured data.

The detector is mounted to a platform that can be rotated, allowing angular positioning relative to the source. The platform can be fixed at increments of 5° .

2.3 Targets

For task 2 and 3, the target was a small aluminum cylinder with a diameter and height of 1 cm. The cylinder was mounted on a plastic stand at the same height as the source.

In task 4, the targets consisted of small rectangular block of aluminum, iron, copper and lead. To prevent direct handling of lead, and additional layer of plastic was put over the block. These targets were placed in a cylindrical holder with a cut-out to ensure stable and consistent positioning during measurements.

3 Execution and evaluation

3.1 Task 1 - Energy calibration and efficiency calculation

3.1.1 Energy calibration

The digitizer records the number of events detected for each channel in a range from 0 to 2000. Since the correlation between the channel number and energy, a calibration is required. This is achieved using the three radioactive isotopes already mentioned. Each source is positioned directly in front of the scintillator to maximize spectral clarity, and measurements are taken over $t_{\text{meas}} = 300$ s, a duration consistent across all subsequent measurements.

The recorded spectra are then read out using a Python program and their respective photopeaks analyzed. The final relationship between n_{channel} and E is obtained by linearly fitting the channels of the photopeaks to their respective channel positions, as shown in Figure 3.2.

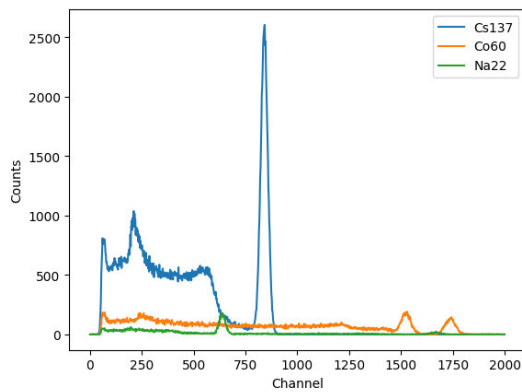


Figure 3.1: Raw Spectra for the different materials used in the calibration.

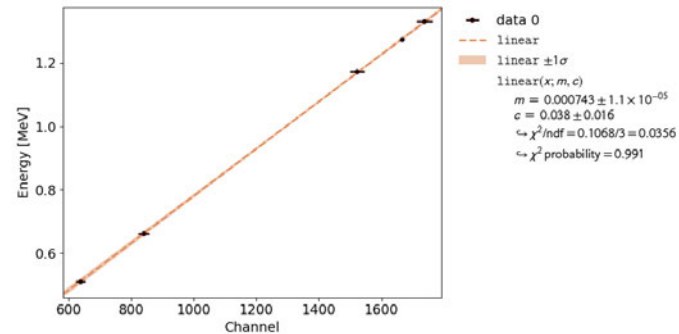


Figure 3.2: The energies plotted against the channels with a linear fit.

The fitting process is performed using the kafe2 Python package, with errors derived from the photopeak fits.

The result is:

$$E(n_{\text{channel}}) = 7.4 \cdot 10^{-4} \cdot n_{\text{channel}} + 3.8 \cdot 10^{-2}. \quad (3.1)$$

This relationship allows subsequent data analysis.

3.1.2 Efficiency calculation

The efficiency ϵ will be calculated with the same data as the calibration. It is given:

$$\epsilon = \frac{N_{\text{ph}}}{t_{\text{meas}} \cdot R_{\gamma}}$$

where N_{ph} is the number of photons in the photopeak and R_{γ} is the γ -ray flux rate.

Determining N_{ph}

N_{ph} is calculated by fitting the photopeak to a Gaussian curve and integrating the resulting curve. This is done for each photopeak resulting in an energy dependency of ϵ .

Determining R_γ

The detector rate R_γ is calculated as:

$$R_\gamma = \Phi_{\text{det}} \cdot F_{\text{Area}} = \Phi_{\text{det}} \cdot \pi r^2$$

where

- $\Phi_{\text{det}} = A_\gamma \cdot \frac{1}{4\pi l^2}$ is the γ -ray flux at the detector,
- $A_\gamma = A_0 e^{-\lambda t_{\text{passed}}}$ is the activity of the source, adjusted for decay,
- $l = 3.3$ cm is the distance from the source to the detector,
- $r = 2.54$ cm is the radius of the scintillator.

The decay constant λ is calculated from the half-time, $\lambda = \ln(2)/t_{1/2}$, and the elapsed time. The source activity was measured on 16 April 2021 and the experiment was done on 25 November 2024, corresponding to $t_{\text{passed}} = 1319$ days = 3.61 a.

Results

The results are shown below:

Probe	A_0 [Bq]	$t_{1/2}$ [a]	R_γ [1/s]	N_{ph}	ϵ
^{137}Cs	$2.8 \cdot 10^5$	30.2	$3.82 \cdot 10^4$	$5.26 \cdot 10^4$	$4.59 \cdot 10^{-3}$
^{60}Co	$6.39 \cdot 10^4$	5.27	$5.88 \cdot 10^3$	$4.79 \cdot 10^3_{\text{peak 1}}$ $3.68 \cdot 10^3_{\text{peak 2}}$	$2.72 \cdot 10^{-3}_{\text{peak 1}}$ $2.09 \cdot 10^{-3}_{\text{peak 2}}$
^{22}Na	$1.1 \cdot 10^4$	2.6	$6.21 \cdot 10^2$	$3.24 \cdot 10^3_{\text{peak 1}}$ $1.79 \cdot 10^2_{\text{peak 2}}$	$1.73 \cdot 10^{-2}_{\text{peak 1}}$ $9.61 \cdot 10^{-4}_{\text{peak 2}}$

The efficiency of the detector varies greatly. This is most likely the fault of l not remaining the same for each probe, the probes not pointing directly at the detector or an inaccurate fit that results in inaccurate values for N_{ph} . Finally, to get a continuous efficiency curve, a quadratic and [cubic interpolation](#) is done. The results are seen in Figure 3.3.

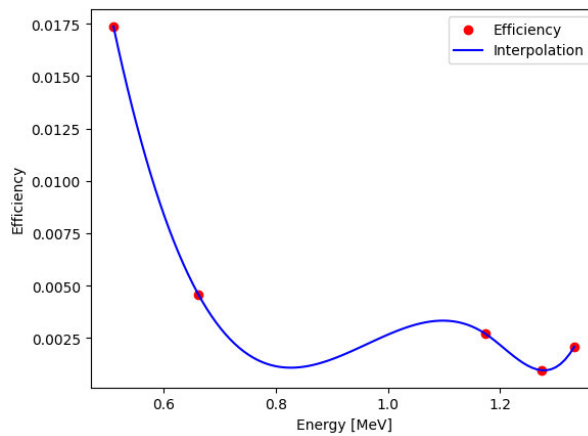


Figure 3.3: The calculated efficiency points at different energies with a quadratic and cubic interpolation.

3.2 Task 2 - Measurement of the differential effective cross section

Once the energy measurements were calibrated and calculated, the next task is to determine the differential cross section $\frac{d\sigma}{d\Omega}$. For this purpose, ^{137}Cs was used as the γ -quanta source, and an aluminum cylinder served as the target. The detector is then observed at a solid angle $\Delta\Omega$ with a mean scattering angle θ . It was then rotated and fixed around the target between $\theta = 30^\circ$ and $\theta = 80^\circ$ in 10° steps. For each angle, two rates were measured: the rate with the aluminum target in place $R_T(\Delta\Omega, \theta)$ and the background rate $R_B(\Delta\Omega, \theta)$ without it. The true rate scattered rate on the aluminum target is given by the difference between the measurements

$$R_{\text{Al}}(\Delta\Omega, \theta) = R_T(\Delta\Omega, \theta) - R_B(\Delta\Omega, \theta). \quad (3.2)$$

$\theta [^\circ]$	30	40	50	60	70	80
$R_{\text{Al}} [\text{s}^{-1}]$	105,41	83,04	64,87	49,46	43,09	39,29

Table 3.1: Scattering rates for different angles

With the true measured rate $R_{\text{Al}}(\Delta\Omega, \theta)$, the gamma quantum flux Φ_γ , and the number of electrons in the target n , the differential cross-section is given by (see Equation 1.9):

$$\frac{d\sigma}{d\Omega} = \frac{R_{\text{Al}}(\Delta\Omega, \theta)}{\Delta\Omega} \cdot \frac{1}{\Phi_\gamma \cdot n} \cdot \frac{1}{\epsilon}, \quad (3.3)$$

whereas ϵ refers to the efficiency calculated in the previous task. However, ϵ was only valid for energy values between 0,511 MeV and 1,332 MeV, while the measured photopeaks fall within 0,285 MeV and 0,523 MeV (see 3.3 Task 3). Therefore, it was decided to proceed using the efficiency value of the lowest energy available within the measured range $\epsilon = 1,73 \cdot 10^{-2}$. To calculate the other constants, different methods are available. In the case of determining the number of electrons in the aluminum target n , the calculation involves

$$n = \frac{N_A}{A_{\text{Al}}} \cdot Z_{\text{Al}} \cdot \rho_{\text{Al}} \cdot \pi r_{\text{Al}}^2 \cdot l_{\text{Al}} \quad (3.4)$$

with Avogadro's number N_A , atomic weight A_{Al} , atomic number Z_{Al} , density ρ_{Al} , radius r_{Al} and length l_{Al} . In order to calculate the gamma quantum flux Φ_γ , the initial flux Φ_0 , measured at the location of the target in June 1971, is used. Therefore, a correction with the time passed since the measurement t_{passed} and the half life $t_{1/2}$ of ^{137}Cs must be applied

$$\Phi_\gamma = \Phi_0 \cdot \exp\left(-\ln(2) \cdot \frac{t_{\text{passed}}}{t_{1/2}}\right). \quad (3.5)$$

Lastly, the solid angle $\Delta\Omega$ can be calculated using the geometry of the experimental setup

$$\Delta\Omega = 2\pi \left(1 - \frac{L}{\sqrt{L^2 + r^2}}\right), \quad (3.6)$$

with the radius of the crystal r and the distance between the target and the detector L . By combining Equations 3.2 to 3.6, the differential cross section for each angle can be calculated. Both the Table 3.2 and the Figure 3.4 reveal that as the angle increases, the differential cross section decreases. This was expected, as larger angles correspond to smaller measured rates. However, when comparing the experimental results with the theoretical values according to

θ [°]	Measured $\frac{d\sigma}{d\Omega}$ [10^{26}cm^{-2}]	Theoretical $\frac{d\sigma}{d\Omega}$ [10^{26}cm^{-2}]	$\frac{\text{Measured}}{\text{Theoretical}}$ []
30	19,94	5,13	3,89
40	15,71	3,89	4,04
50	12,27	2,90	4,23
60	9,36	2,21	4,24
70	8,15	1,75	4,65
80	7,43	1,47	5,04

Table 3.2: Comparison between measured and theoretical differential cross section

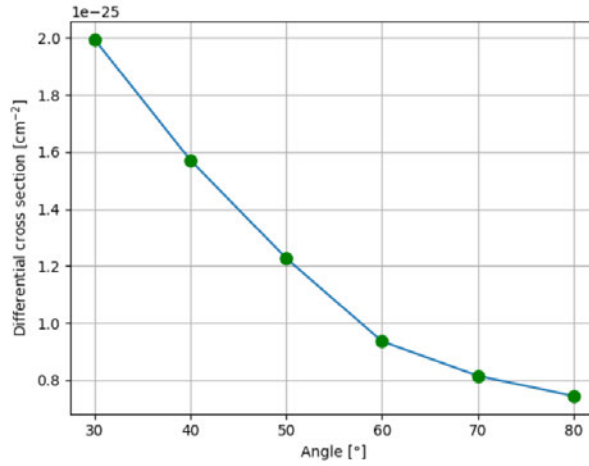


Figure 3.4: Plot of the differential cross section against the angle

Klein-Nishina [Wol24], the experimental results are consistently larger by a factor ranging from 3.89 to 5.04. This factor increases with the scattering angle. This discrepancy is likely due to the efficiency ϵ . In the first task, the efficiency measurements did not yield a constant result, and the interpolation only provided values for a limited range, which did not cover most of the measured energies.

3.3 Task 3 - Measurement of the energy shift and estimation of the rest energy of the electron

The next objective is to determine the Compton shift as a function of the scattering angle θ the electron rest energy $E_0 = m_0c^2$. This analysis utilized the same measurements performed for the differential cross section, following an identical procedure with the same source and target. The photopeaks were identified in the spectra, and their corresponding energies were recorded. The conversion from channel numbers to energy was performed using the equation 3.1.

θ [°]	30	40	50	60	70	80
E' [MeV]	0.523	0.466	0.413	0.363	0.324	0.285

Table 3.3: Photon energy after collision for different angles

A clear inverse relationship between energy and angle can be identified in Table 3.3 and Figure 3.5. This indicates that as the angle increases, more energy is transferred to the electron, and the photon's energy after the collision decreases. This behavior aligns with the expected theoretical

prediction (see Theoretical Principles 1.1). The next step involves performing a fit to calculate the electron's rest energy. The model function used for this purpose is derived by rearranging Equation 1.3

$$\frac{1}{E'} = \frac{1}{E} + \frac{1 + \cos \theta}{E_0}.$$

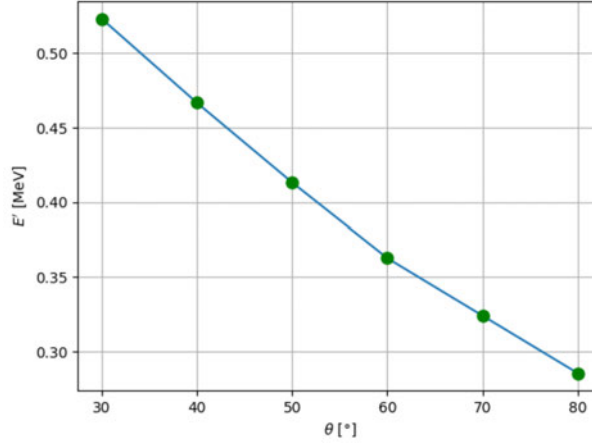


Figure 3.5: Plot of the photon energy after collision against the angle

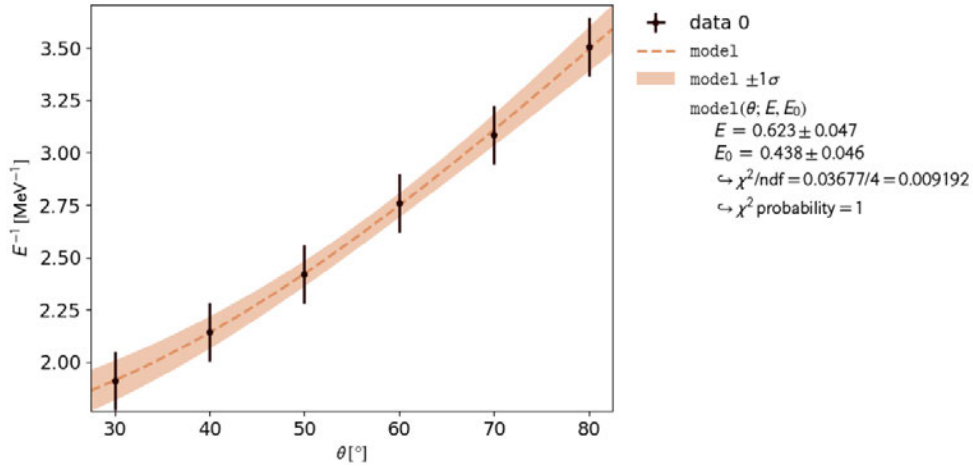


Figure 3.6: Fit of the energy against the angle with the model function

As a result, the rest energy of the electrons is determined to be $E_0 = m_0c^2 = (0,438 \pm 0,046)$ MeV (see Figure 3.6), which is quite close to the theoretical value $E_{0, \text{theoretical}} = 0,511$ MeV, though it does not fall within the given uncertainty. Similarly, the estimated value for the original photon energy is $E = (0,623 \pm 0,047)$ MeV, which should correspond to the energy of the Cesium photopeak $E_{137\text{Cs}} = 0,662$ MeV. In this case, the result is relatively close and includes the theoretical value within its uncertainty. The fit was done with the kafe2 package in Python and the aforementioned errors in the fit results stem from deviations in the channel-to-energy transformation calculated in the first task.

3.4 Task 4 - Measurement of the dependence of the effective cross section on the atomic number

The previous analysis of the differential cross section referred to a single electron that is assumed to be free and at rest. However, when comparing different materials to each other, the entire atom is of interest. To achieve this, each material will be placed in front of the γ -source and their respective spectra will be measured. This measurement was taken at an arbitrary angle, $\vartheta = 50^\circ$, relative to the source. In addition to these spectra, one background spectrum was taken to account for background radiation.

Assuming all electrons in the atom are independent and the γ -energy is large enough compared to the binding energies, the following equation should hold true.

$$\left(\frac{d\sigma}{d\Omega}\right)_a = Z \left(\frac{d\sigma}{d\Omega}\right)_e$$

where Z is the atomic number and a and e are referring to the differential cross section of the atom and electron respectively. Using the equations 3.3 and 3.4 for the respective material, one gets:

$$\left(\frac{d\sigma}{d\Omega}\right)_e = \frac{R}{\Delta\Omega} \frac{1}{\Phi_0 \epsilon} \frac{1}{\frac{N_A}{A} Z \rho \pi \left(\frac{d}{2}\right)^2 l} = C \cdot R \frac{A}{\rho Z}$$

where C is a quantity independent of the target material. If the assumption made earlier holds true, the quantity $R \frac{A}{\rho}$ plotted against the corresponding atomic number should be a straight line. Another possibility is to plot the quantity $R \frac{A}{\rho Z}$ over the atomic number, which is more sensitive to deviations. This plot should be a constant line parallel to the axis of the atomic number.

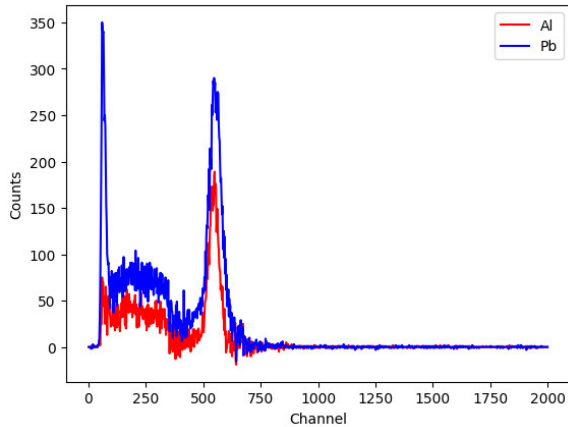


Figure 3.7: Spectrum of ^{137}Cs with Al and Pb in front of the source.

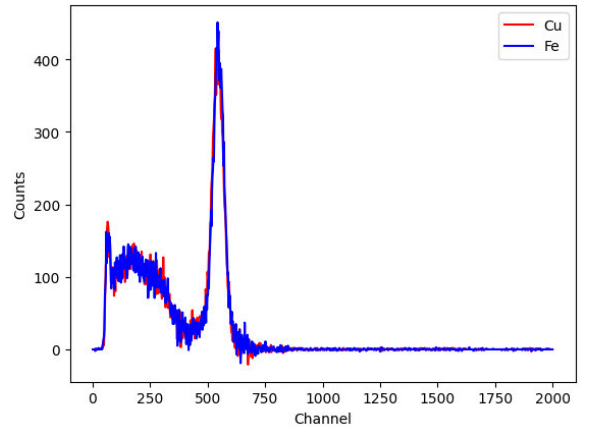


Figure 3.8: Spectrum of ^{137}Cs with Cu and Fe in front of the source.

After calculating the respective rates, it is possible to evaluate $f_1 = R \frac{A}{\rho}$ and $f_2 = R \frac{A}{\rho Z}$ using the known values for A , Z and ρ .

Results

As shown in Figure 3.9, the **expected linear relation** is approximately given. As seen in Figure 3.8, both the Fe and Cu spectrum are almost identical leading to almost identical values in Figure 3.9. In figure 3.10 the more sensitive function f_2 is plotted against Z . A downwards trend is depicted. This deviation is relatively small and only changes 9 units over a range of $Z = [13, 82]$. This can be attributed to a non optimal placement and the impurity of the materials. For example, lead had a thin plastic layer in order to prevent contact with the skin.

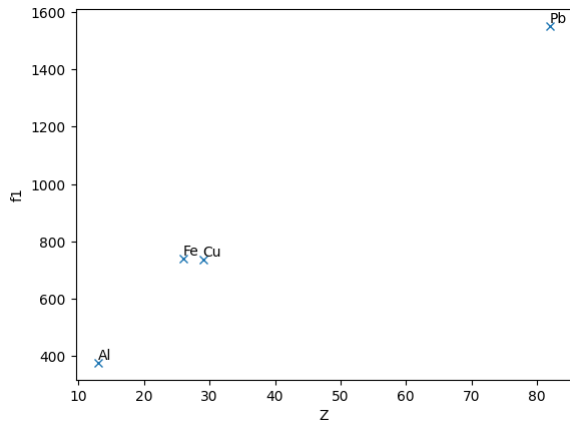


Figure 3.9: The function $f_1 = R \frac{A}{\rho}$ over the respective atomic numbers.

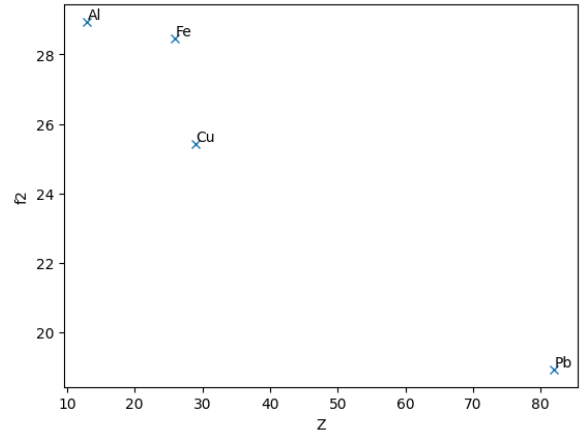


Figure 3.10: The function $f_2 = R \frac{A}{\rho Z}$ over the respective atomic numbers.

Sources

[Wol24] WOLF, Joachim: *Introduction to the Nuclear and Particle Physics Lab Course*. KIT, 2024